Multimode Parameter Extraction for Multiconductor Transmission Lines via Single-Pass FDTD and Signal-Processing Techniques

Yuanxun Wang, *Student Member, IEEE,* and Hao Ling, *Senior Member, IEEE*

***Abstract*— We present two approaches to extract the broad-band multimode parameters of guided wave structures from a single-pass finite-difference time-domain (FDTD) simulation. They include a two-dimensional (2-D) Fourier transform (FT) algorithm and a super-resolution estimation of signal parameters via rotational invariance technique (ESPRIT) algorithm. Comparison is made to show the superiority of the super-resolution approach. As a typical application, a three-line coupled microstrip structure is studied. After a single-pass FDTD simulation, broad-band multimode parameters such as propagation constants, modal-field templates, and modal impedances are extracted and verified against published data obtained by the spectral-domain method. The main feature of this parameter-extraction methodology is that it decouples the computational electromagnetics engine (in this case, the FDTD simulator) from the post-processing parameter-extraction algorithm, thus providing more flexibility and connectivity among the various simulation tools.**

***Index Terms*—FDTD, parameter extraction, super resolution.**

I. Introduction

THE finite-difference time-domain (FDTD) method has been extensively used as a flexible and accurate way to predict the electromagnetic behaviors of various guided wave structures in monolithic microwave integrated circuits (MMIC's). The most important feature of the FDTD method is that broad-band frequency information can be provided in a single-pass simulation. Since the results directly produced by an FDTD run are time-domain data, which contain multiple frequency and mode contents, the extraction of desired frequency parameters from these data becomes an important issue.

The earliest work of using a single-pass FDTD for guided wave problems is that of Zhang *et al.* [1], who proposed a simple Fourier transform (FT) method to obtain the dispersion curve of a microstrip line for its dominant quasi-TEM mode. However, this type of processing method is limited to single mode data and is no longer valid when higher modes exist. The works described in [2] and [3] employed a two-dimensional (2-D) FDTD method to obtain multimode dispersive characteristics. Since only those frequency data corresponding to an assumed phase constant can be obtained from one FDTD run in this approach, the FDTD simulation itself must be repeated many times to generate broad-band information. Paul *et al.* [4] presented a technique combining the two methods above to extract multimode broad-band parameters. First, the 2-D FDTD method is used to generate the field template for each mode at a single frequency. This field template is then used as an excitation to maintain single-mode propagation, as required by the method of [1]. The limitation of this method is that the field templates are assumed to be frequency invariant.

In this paper, we present two approaches to extract broad-band multimode parameters of guided wave structures from a single-pass FDTD simulation. The first approach is a 2-D FT method. We demonstrate the effectiveness of this approach by extracting the multimode information in the ω–β plane for a single-conductor microstrip line. While this method is simple and straightforward, it is limited in resolution by Fourier constraints. For example, this approach fails to resolve the three quasi-TEM modes of a coupled three-line microstrip where the dispersion curves are very close to each other. Accurate values of the dispersion characteristics cannot be obtained due to the Fourier limit, unless an extremely long simulation domain is used. In the second approach, a super-resolution algorithm is employed in the spatial dimension in place of the Fourier engine to overcome this difficulty. In the past, super-resolution algorithms such as Prony's method have in fact been used to extract the scattering parameters for discontinuity problems and to correct the errors due to imperfect absorbing-boundary condition [5], [6]. Here, we follow the same spirit, but extend this technique to extract the multimode parameters for general multiconductor transmission lines. Instead of Prony's method, the estimation of signal parameters via rotational invariance technique (ESPRIT) [7] algorithm is used because it is considered to have more stability (with respect to noise). We demonstrate the superiority of this second approach by computing (after a single-pass FDTD run) the broad-band characteristics of a three-line coupled microstrip structure. The resulting propagation constant and modal impedance data for the quasi-TEM modes are compared with published data obtained by the spectral-domain method

Manuscript received August 26, 1997; revised October 9, 1997. This work was supported by the Joint Services Electronics Program under Contract AFOSR F49620-95-C-0045, and in part by the U.S. Air Force MURI Center for Computational Electromagnetics under Contract AFOSR F49620-96-1-0025.

The authors are with the Department of Electrical and Computer Engineering, The University of Texas at Austin, Austin, TX 78712-1084 USA.

Publisher Item Identifier S 0018-9480(98)00624-3.

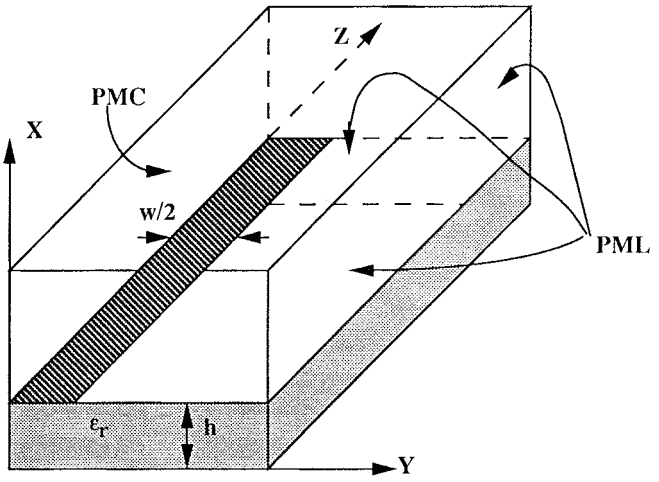

Fig. 1. FDTD model for an open single-line microstrip with $W/h = 2.0$, $h = 1.0$ mm, $\varepsilon_r = 13.0$.

to verify this approach. In addition, we generate the broadband modal-field templates to obtain further insights into the underlying physical phenomenology.

II. 2-D FT Method

We shall present the first approach through an example which extracts the multimode characteristics of an open single-line microstrip. The structure is shown in Fig. 1 with parameters $w/h = 2.0$, $h = 1.0$ mm, and $\varepsilon_r = 13.0$. In our FDTD simulation, Berenger's perfectly matched layer (PML) absorbing-boundary condition [8], [9] is implemented on both the sidewalls and the endwall of the problem domain to simulate the open microstrip structure. We find that the side absorber must be carefully chosen to make the reflection as small as possible, as it can have strong influence on the computed dispersion parameters. Although the error due to the reflection from the end of microstrip can be corrected by using the method of [5] and [6], the side absorber reflection must be carefully minimized. A perfectly magnetic conducting (PMC) wall is used along the symmetry plane when considering the even modes. To properly excite all the higher order modes in the FDTD simulation, a spatially singular δ-source is placed just beneath the strip. The input signal is a Gaussian pulse in time. The total FDTD mesh consist of $65 \times 46 \times 176$ cells, which includes the PML absorbers.

As we have mentioned in Section I, the simple one-dimensional (1-D) FT method proposed in [1] is not applicable to the multimode case, because the resulting data are not only frequency mixed, but also mode mixed. One solution is to utilize the whole collection of time data taken along the z-direction and carry out a 2-D FT to obtain the desired ω–β spectra. Note that the signal simulated by the FDTD algorithm can be expressed as $f(t, x, y, z)$, where z is the propagation direction. By choosing a fixed (x_0, y_0) observation along every cross section of the waveguide, we can define the signal as a 2-D function $f(t, z)$, which is expressible as a 2-D Fourier integral as follows:

$$f(t, z) = \int_{-\infty}^{\infty} \int_{-\infty}^{\infty} F(\omega, \beta) e^{j(\omega t - \beta z)}\, d\omega\, d\beta. \qquad (1)$$

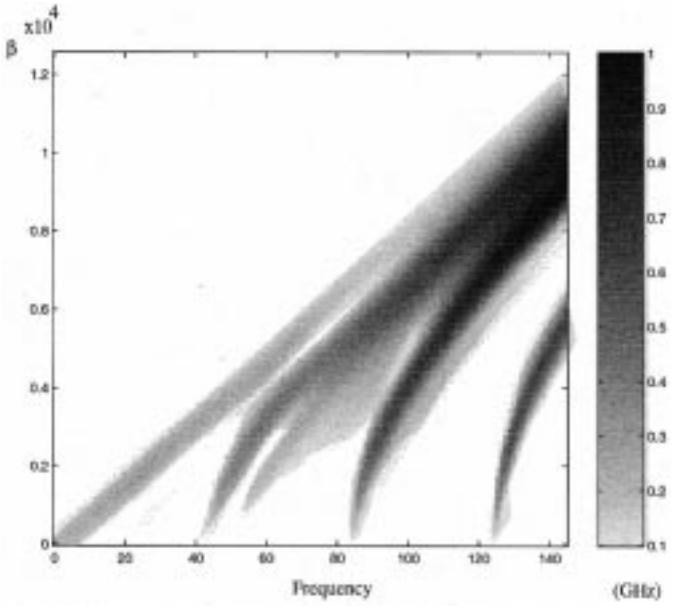

Fig. 2. The ω–β spectra obtained by using the 2-D FFT algorithm.

If we assume that only discrete guided modes are present in the signal, $f(t, z)$ should take on the form

$$f(t, z) = \int_{-\infty}^{\infty} \sum_i ai(\omega)\, e^{j[\omega t - \beta i(\omega) z]}\, d\omega \qquad (2)$$

where the summation is taken over all the discrete modes and $a_i(\omega)$ is the frequency-dependent amplitude of each mode. Therefore, by taking the 2-D FT of the signal $f(t, z)$, we should obtain the discrete ω–β spectra in the form of

$$F(\omega, \beta) = \sum_i a_i(\omega) \delta[\beta - \beta_i(\omega)]. \qquad (3)$$

$\beta_i(\omega)$ versus ω is the desired dispersion curve for mode i. To get this ideal dispersive curve with infinite resolution, infinite time, and infinite long simulation domain are required. For truncated time and longitudinal data, a fuzzy image for the dispersion curves is obtained by using a 2-D fast FT (FFT) algorithm, where the resolution are limited by $\Delta\omega = 2\pi/t_{\max}$, $\Delta\beta = 2\pi/z_{\max}$. To avoid aliasing, the z-direction sampling interval must be smaller than half of the minimum waveguide wavelength. Moreover, in order to reduce the sidelobe caused by the truncation, a windowing operation should be applied to the longitudinal data prior to the FFT.

Fig. 2 shows the dispersion curves obtained using the 2-D FFT approach. From it, we can clearly see five mode spectra being revealed in the ω–β plot. The intensity of these dispersion curves is dependent on the spatial distribution of the excitation. The nearly linear dispersion curve starting from zero frequency corresponds to the dominant quasi-TEM mode. The other four lines represent the four higher order even modes in the microstrip (since the problem is simulated using a PMC symmetry plane). Their cutoff frequencies are 43, 52, 84, and 124 GHz. If we repeat this operation at all the grid points over the cross section, the field-distribution template for each mode can also be obtained. Both the effective dielectric constant for the dominant TEM mode and the modal templates for the

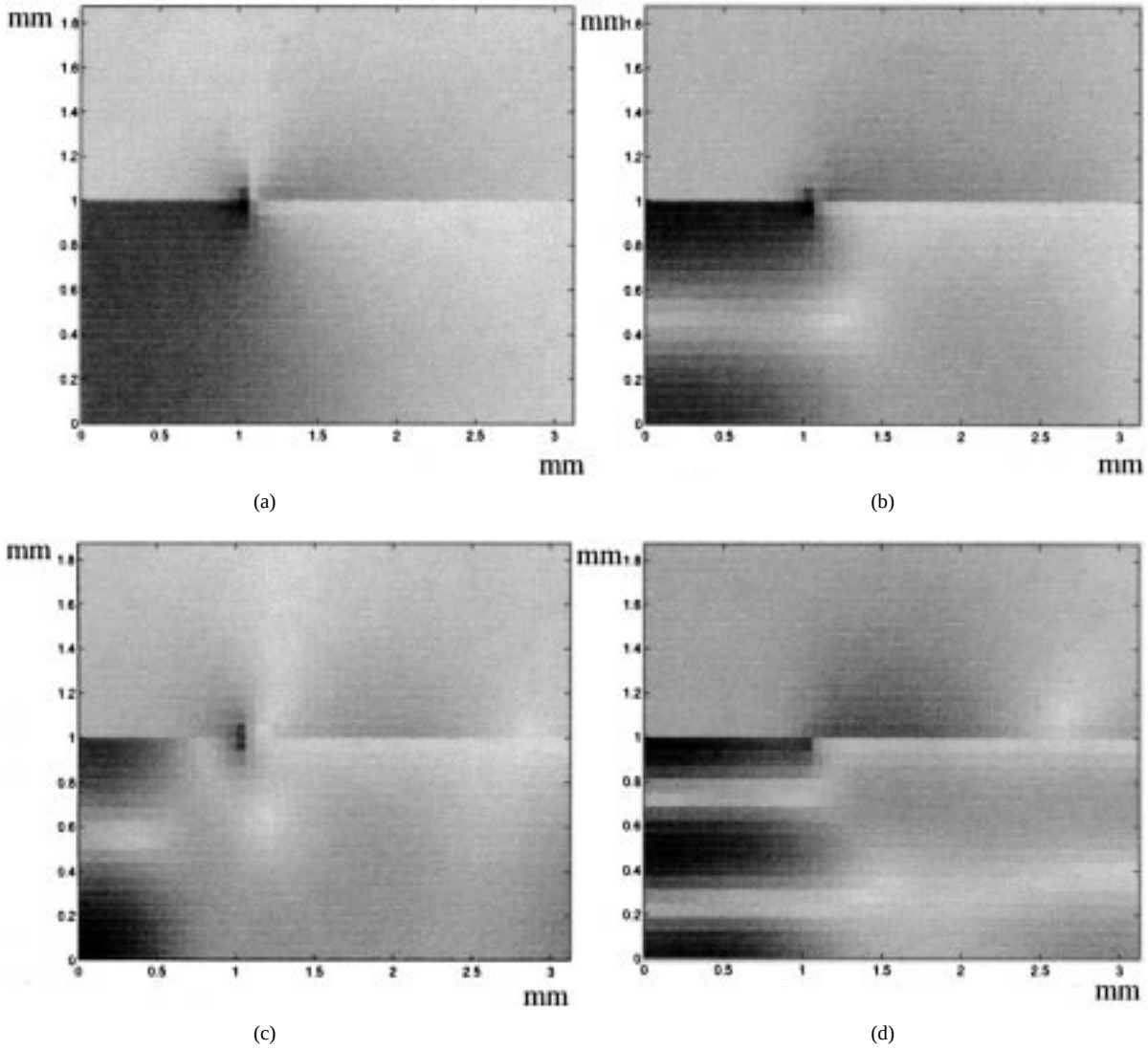

Fig. 3. The spatial field distribution extracted for the first four even modes. (a) Dominant mode at 20 GHz. (b) First higher order even mode at 46 GHz (cutoff = 43 GHz). (c) Second higher order even mode at 54 GHz (cutoff = 52 GHz). (d) Third higher order even mode at 87 GHz (cutoff = 84 GHz).

higher order modes have been reported earlier in [10] and [11]. Here we plot the modal E_x-field templates for the four lowest even modes in Fig. 3. We observe that the modal fields' distributions are fairly well confined under the microstrip and exhibit the characteristic spatial variations of the higher order modes.

As a second example, we study an asymmetric three-line coupled microstrip. The geometry is shown in Fig. 4. We choose the same physical parameters as those used in [12] for later comparison, viz $W_1 = 0.3$ mm, $S_1 = 0.2$ mm, $W_2 = 0.6$ mm, $S_2 = 0.4$ mm, $W_3 = 1.2$ mm, $h = 0.635$ mm, $\varepsilon_r = 9.8$. The total FDTD simulation domain consists of $24 \times 59 \times 816$ cells, including 8, 16 (two sides), and 16 layers of PML absorber cells in the x-, y-, and z-directions, respectively. A Gaussian pulse is used as excitation which only exists spatially beneath the first line. The ω–β plot of using the 2-D FFT algorithm is shown in Fig. 5. According to the electrostatic theory, there must be three quasi-TEM modes for a three-conductor transmission line. However, due to the limited resolution of the 2-D FT algorithm, only two curves in the ω–β plane can be seen. The 2-D FFT algorithm fails to resolve the closely spaced spectra. One solution is to use a much longer simulation domain, which means a large amount of computer resources is required. Next, we present a super-resolution algorithm to overcome this difficulty.

III. Super-Resolution Algorithm

In order to overcome the Fourier resolution limit, we shall replace the Fourier engine by super-resolution processing in the spatial dimension to better resolve β. We first take the 1-D FT signal $f(t, z)$ with respect to time to generate the function $\tilde{F}(\omega, z)$. As we can readily see from (3), $\tilde{F}(\omega, z)$ can be expressed as a discrete sum of exponentials in z for a guided wave signal

$$\tilde{F}(\omega, z) = \sum_{i=1}^{d} a_i(\omega)\, e^{-j\beta_i(\omega) z} \tag{4}$$

where d is the number of modes in the signal. Any number of super-resolution algorithms can now be used to determine

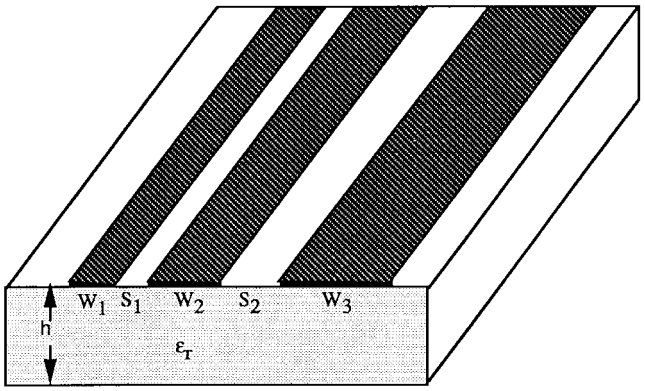

Fig. 4. Geometry of a general three-line coupled microstrip line.

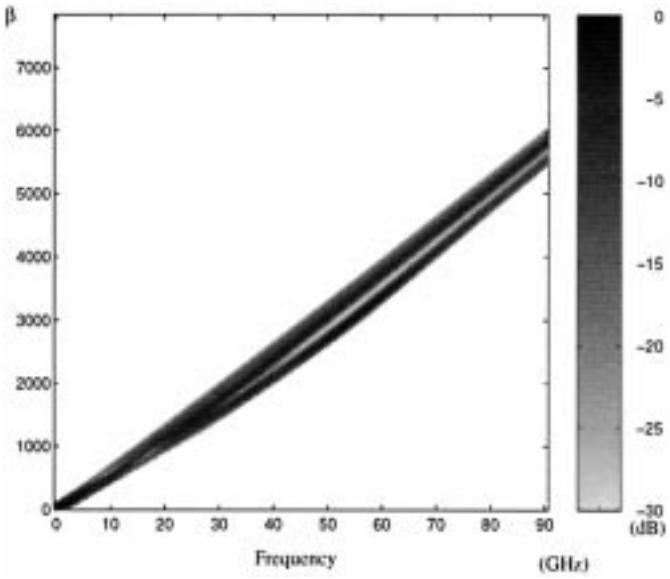

Fig. 5. The ω–β spectra obtained by using the 2-D FFT algorithm for an asymmetric three-line coupled microstrip with $W_1 = 0.3$ mm, $S_1 = 0.2$ mm, $W_2 = 0.6$ mm, $S_2 = 0.4$ mm, $W_3 = 1.2$ mm, $h = 0.635$, $\varepsilon_r = 9.8$.

$\beta_i(\omega)$ from spatial samples of $\tilde{F}$ in z. Note that this should be done for each frequency ω to map out the entire dispersion spectra. We will choose the super-resolution algorithm ESPRIT due to its robustness in the presence of noise. It was originally developed for direction-finding applications and has been used by us for radar feature extraction [13]. ESPRIT is based on the data model as follows:

$$\tilde{F}(z_k) = \sum_{i=1}^{d} a_i e^{-j\beta_i z_k} + n(z_k), \qquad z_k = z_1, z_2, \cdots, z_N \tag{5}$$

where $n(\bullet)$ denotes additive white Gaussian noise. If the data sequence obeys this ideal model exactly and the number of the sampling points $N > 2d+1$, ESPRIT can estimate d and resolve each β_i and a_i without any error.

After running ESPRIT for each frequency, the values of the modal amplitude $a_i(\omega)$ and phase constant $\beta_i(\omega)$ can be calculated to construct the dispersion spectra over a broad frequency band. Fig. 6 shows the results for the asymmetric three-line coupled microstrip discussed in Fig. 5. Comparing Fig. 6 to

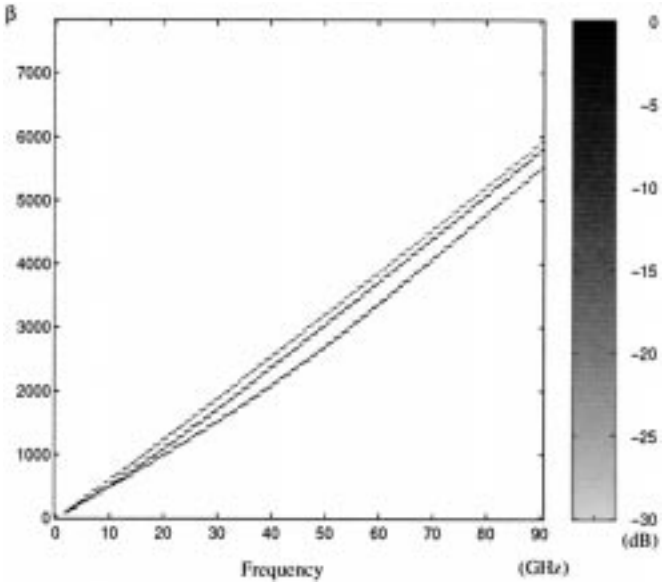

Fig. 6. Super-resolved ω–β spectra obtained by using the ESPRIT algorithm for the same structure as in Fig. 5.

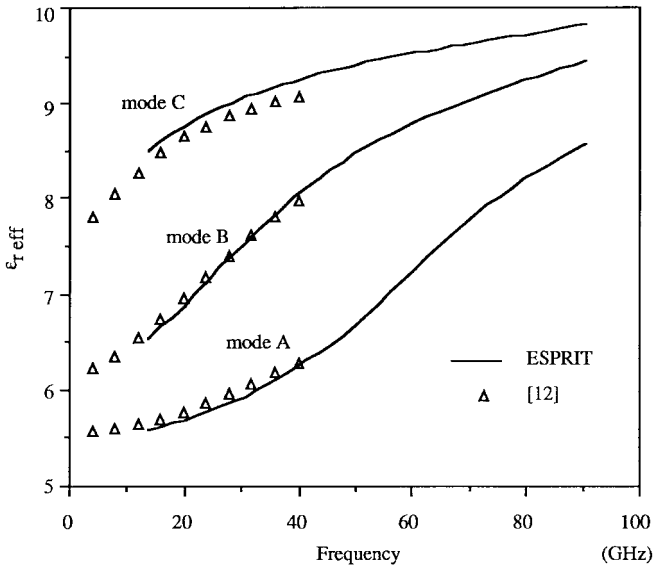

Fig. 7. The effective dielectric constants versus frequency plots for the three quasi-TEM modes in the asymmetric three-line coupled microstrip from Fig. 6.

Fig. 5, we see that the three dominant quasi-TEM modes are now clearly resolved by the super-resolution approach using the same set of simulation data. The effective dielectric constant curves are also generated from the dispersion curves and are shown in Fig. 7. They agree well with the spectral-domain results of [12]. It is worthwhile to point out that ESPRIT still has difficulty extracting the parameters at very low frequencies. We believe this is due to a combination of two reasons. One reason is that the FDTD simulation data are not noise-free, and numerical error does not necessarily behave like white noise. Thus, the resolution of ESPRIT is not infinite anymore, but rather becomes limited by the length of the simulation domain and the signal-to-noise ratio. The other reason is that the propagation constants of all modes approach

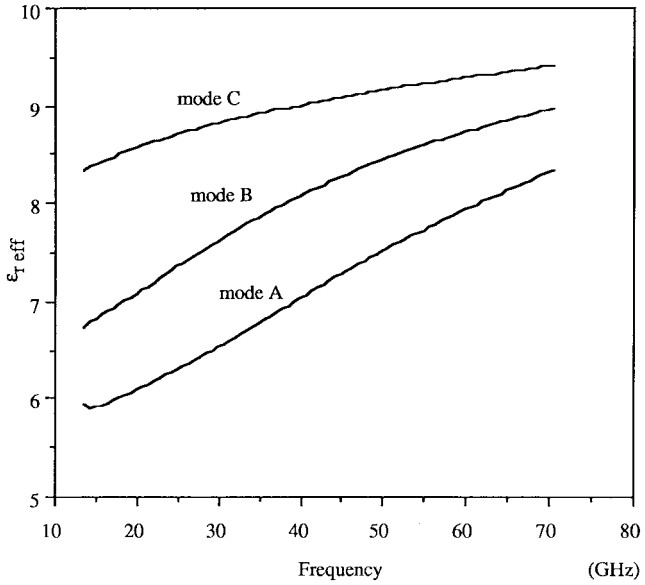

Fig. 8. The effective dielectric constant versus frequency plots for the three quasi-TEM modes in the symmetric three-line coupled microstrip ($W_1 - S_1 = W_2 = S_2 = W_3 = 0.6$ mm, $h = 0.635$ mm, $\varepsilon_r = 9.8$).

zero when frequency tends to dc. Thus, resolving these closely spaced modes becomes quite challenging for ESPRIT at low frequencies. One effective way to improve the results in the low-frequency range is to divide the total frequency range into two or more subbands and running FDTD for each subband. For the low frequency band, a coarser FDTD cell division can be used. This way, the simulation domain can be lengthened without increasing the memory requirement.

Next, we will extract other important parameters including modal-field templates and modal impedances of the multiconductor line. To determine the modal-field templates, we can simply run the ESPRIT algorithm at every position (x, y) on the cross section of the waveguide to find $a_i(\omega, x, y)$—the modal-field distribution for the ith mode at frequency ω. However, this is time-consuming and not necessary once the propagation constants $\beta_i(\omega)$ are known. Instead, we can simply set up the linear system of equations for each point (x, y):

$$\tilde{F}(\omega, x, y, z_j) = \sum_{i=1}^{d} a_i(\omega, x, y)\, e^{-j\beta_i(\omega) z_j}, \qquad j = 1, 2, 3, \cdots \quad (6)$$

and use a minimum least-square algorithm to solve for $a_i(\omega, x, y)$. To demonstrate the extracted modal-field distribution using this procedure, we will use the more intuitive example of a symmetric coupled microstrip instead of the asymmetric case discussed thus far. Fig. 8 is the effective dielectric constant curve for a symmetrical three-line coupled microstrip with $W_1 = S_1 = W_2 = S_2 = W_3 = 0.6$ mm, $h = 0.635$ mm, $\varepsilon_r = 9.8$. The modal templates for the E_x field at $f = 28$ GHz are shown in Fig. 9(a)–(c), which correspond to modes A, B, and C, respectively. We can identify the "$+\ -\ +$" variation for mode A, "$+\ 0\ -$" variation for mode B, and "$+\ +\ +$" variation for mode C. Although these figures show only the intensity plot, one can identify the

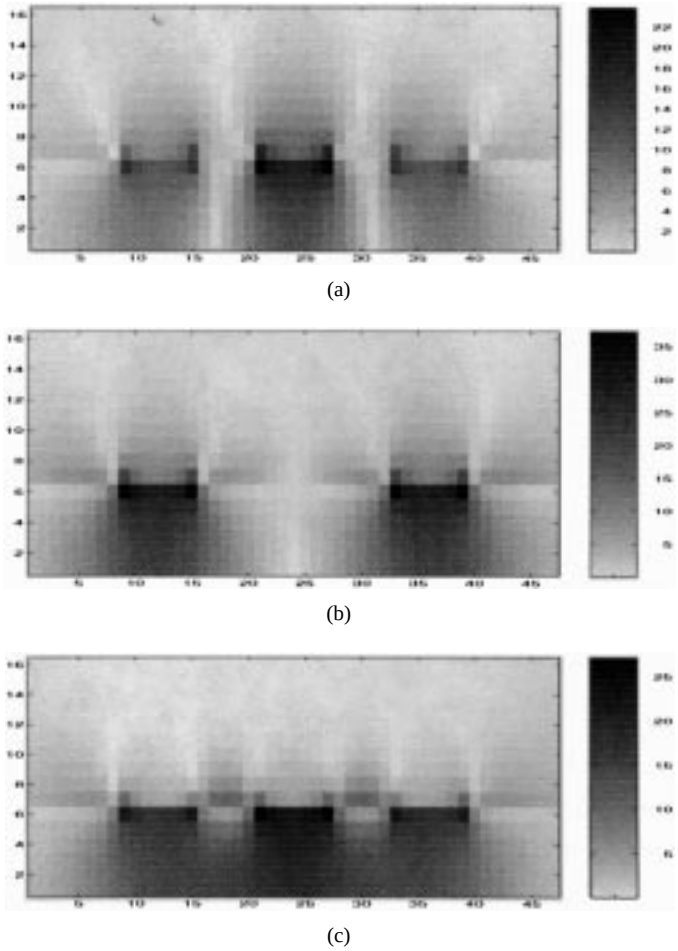

(a)

(b)

(c)

Fig. 9. The E_x field templates for the three quasi-TEM modes in the symmetric three-line coupled microstrip at $f = 28$ GHz. (a) Mode A ($+\ -\ +$). (b) Mode B ($+\ 0\ -$). (c) Mode C ($+\ +\ +$).

polarity by observing that there are two zero crossings in the gap regions for mode A, while there are no zero crossings in the gap regions for mode C. These field variations are similar to those reported in [15] for a symmetric three-line microstrip on a lossy semiconductor substrate. For this example, the FDTD simulation time is approximately 10 h on a single-node SGI R8000 workstation. The post-processing using the super-resolution algorithm takes only a few minutes on the same workstation. Thus, compared to the electromagnetic simulation time, the computer time for post-processing is nearly negligible. The 2-D FFT post-processing algorithm described earlier takes even less time than the super-resolution scheme. However, it requires a much larger simulation domain to achieve the needed resolution, and, therefore, would lead to a much longer electromagnetic simulation time.

To determine the modal impedances of the multiconductor line, we must properly define their meaning. Unlike the static case, the voltage and current definitions in a full-wave model is ambiguous and there are several different definitions presented in the literature. A simple voltage–current definition for the impedance where the voltage is defined as the line integral of electric field in the center of strip and the current is the total z-directed conduction current is used in [14], and [15] and [16] also used a voltage–current definition. However,

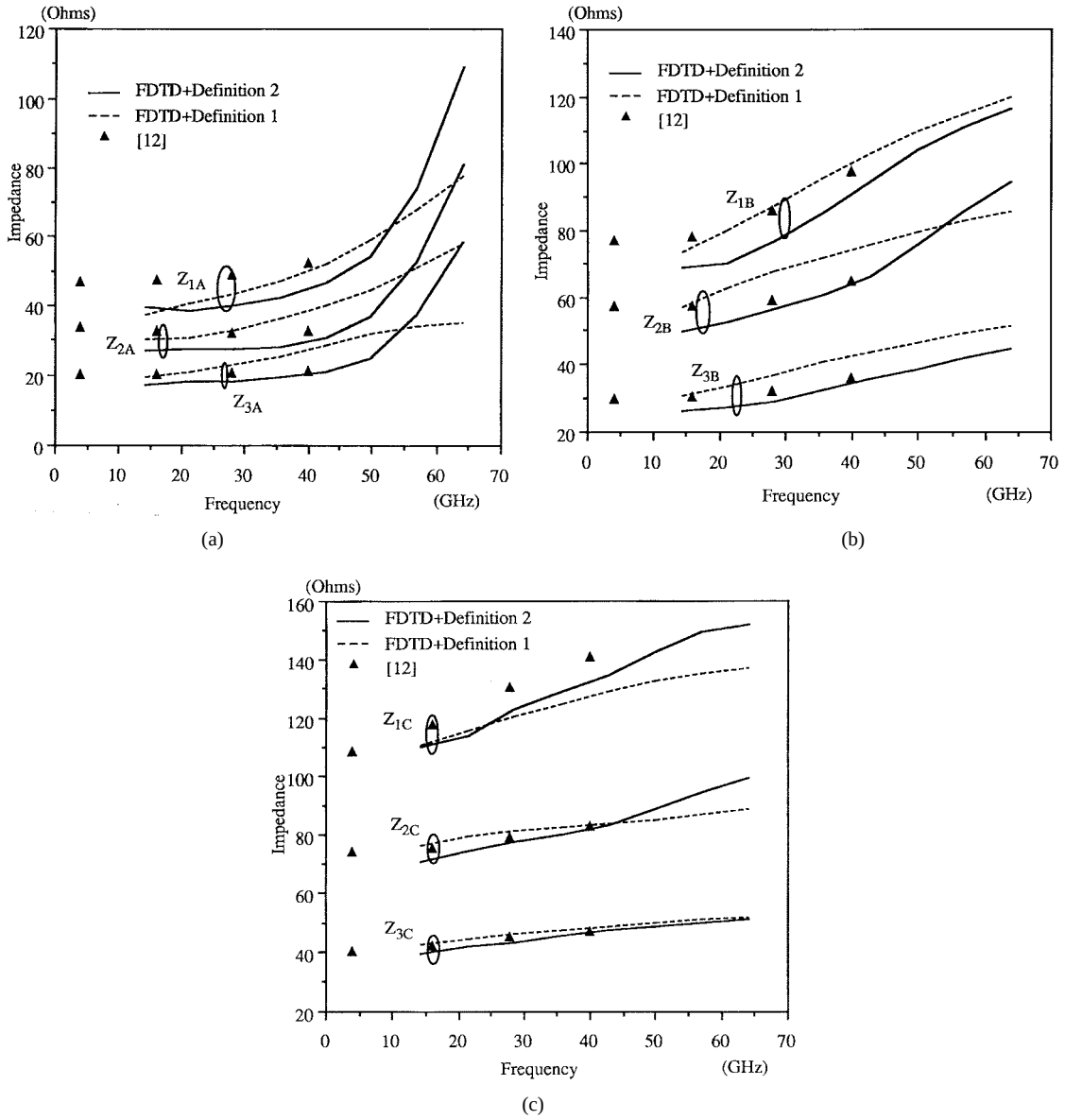

Fig. 10. (a) Line impedances versus frequency for mode A in the asymmetric three-line coupled microstrip. (b) Line impedances versus frequency for mode B in the asymmetric three-line coupled microstrip. (c) Line impedances versus frequency for mode C in the asymmetric three-line coupled microstrip.

instead of arbitrarily choosing a line integral as the voltage, the line–mode voltage matrix is derived by solving the following linear equations:

$$\left.\begin{aligned} P_k &= \tfrac{1}{2} V_k \bullet I_k^* \\ 0 &= \bar{V}_l \bullet I_m (l \neq m) \end{aligned}\right\}, \qquad k, l, m = 1, \cdots, N_{\text{modes}}. \quad (7)$$

In [7], P_k is the power flow of the kth mode. The first equation represents the power condition, and the second equation arises from the reciprocity properties of the multiconductor system. Since the modal power flow and the total z-directed current are both uniquely determined quantities from the modal fields, this definition is considered to have a clearer physical meaning.

Here, both the definition in [14] (definition one) and that in [15] and [16] (definition two) are utilized to compute the modal impedances. The modal impedance curves are plotted in Fig. 10(a)–(c) for the asymmetric geometry discussed earlier. Also plotted for comparison are the results from the spectral-domain calculation of [12], which uses yet a third definition of impedance that allocates the power flow to individual strips. Definitions one and two are expected to give similar impedance estimates when the frequency is low. Indeed, our results in Fig. 10 show this trend. For high frequencies, the discrepancies between the two definitions become much more obvious, as expected. Note that the results using definition two always appear a little bit smaller than those computed using definition one—even for low frequencies. This can be understood from our FDTD modeling. In the FDTD model, the PML absorber is placed close to the side of the strip to simulate the open structure while keeping the computation domain as small as possible. Thus, when we integrate the field distribution over the cross section, we tend to underestimate the total power flow since we have no access to the actual field outside the computation domain. Although this is relatively small compared to the total power flow, it makes the calculated impedance smaller than the correct value.

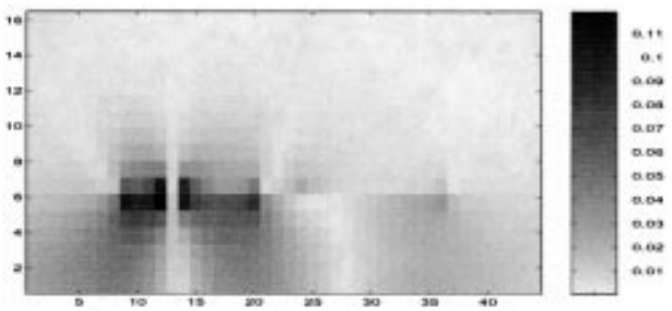

(a)

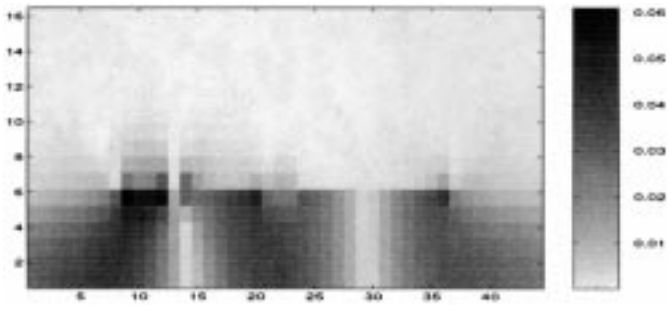

(b)

Fig. 11. The field templates for mode A in the asymmetrical three-line coupled microstrip at (a) $f = 42$ GHz and (b) $f = 64$ GHz.

One interesting phenomenon is observed from Fig. 10(a) when the frequency is higher than 40 GHz. The values of the three line impedances for mode A based on definition two dramatically increase, while the results using definition one—the simple voltage–current definition—do not show this strong upward trend. It is hard to determine which one is more reasonable until further information is provided. To explore the underlying physical phenomenology, we plot the modal E_x-field templates for mode A at both $f = 46$ GHz and $f = 64$ GHz in Fig. 11(a) and (b). Unlike the other two modes, these two modal-field templates for mode A look very different from each other. The field structure at $f = 64$ GHz obviously can carry much more power than the one at $f = 46$ GHz with the same magnitude of currents. Hence, the observed strong frequency variation of impedances using definition two can be attributed to the strong frequency dependence of the field templates for mode A. For the simple voltage–current definition (since the centers of the strips are not where fields are concentrated), it fails to properly reflect this frequency variation. Therefore, we can conclude that definition two employed in [15] and [16] is more representative of the actual physical phenomenology.

IV. Conclusions

Two approaches to extract the broad-band multimode parameters of guided wave structures from a single-pass FDTD simulation have been presented. They include a 2-D FT algorithm and a super-resolution ESPRIT algorithm. As a typical application, a three-line coupled microstrip structure is studied. Comparison is made to show the superiority of the super-resolution approach. After a single-pass FDTD simulation, those multimode parameters such as propagation constants, field templates, and modal impedances are easily obtained by using the ESPRIT algorithm as the post-processing engine.

In view of the flexibility of the FDTD method, there should be no intrinsic limitation to extend this methodology to general multimode guided wave systems. The main feature of this methodology is that it decouples the computational electromagnetic engine (in this case, the FDTD simulator) from the post-processing parameter-extraction algorithm, thus providing more flexibility and connectivity among the various simulation tools. On the other hand, the drawback of this method is that it requires large computer memory to store all the 3-D nodal field values from the FDTD simulation. For the case where the dispersion characteristics are very close to each other for different modes, a relatively long simulation domain is needed, which also makes the computation more intensive.

Acknowledgment

The authors would like to thank Prof. J. Fang of the State University of New York (SUNY) at Binghamton, for information on the PML absorber. The ESPRIT algorithm was provided by Dr. L. C. Trintinalia, formerly of The University of Texas at Austin.

References

[1] X. Zhang, J. Fang, K. K. Mei, and Y. Liu, "Calculations of the dispersive characteristics of microstrip by the time-domain finite difference method," *IEEE Trans. Microwave Theory Tech.*, vol. 36, pp. 263–267, Feb. 1988.

[2] S. Xiao, R. Vahldieck, and H. Jin, "Full-wave analysis of guided wave structures using a novel 2-D FDTD," *IEEE Microwave Guided Wave Lett.*, vol. 2, pp. 165–167, May 1992.

[3] V. J. Brankovic, D. V. Krupezevic, and F. Arndt, "An efficient two dimensional graded mesh finite-difference time-domain algorithm for shielded or open waveguide structures," *IEEE Trans. Microwave Theory Tech.*, vol. 40, pp. 2272–2277, Dec. 1992.

[4] D. L. Paul, N. M. Pothecary, and C. J. Railton, "Calculation of the dispersive characteristics of open dielectric structures by the finite-difference time-domain method," *IEEE Trans. Microwave Theory Tech.*, vol. 42, pp. 1207–1212, July 1994.

[5] K. Naishadham and X. P. Lin, "Application of spectral domain Prony's method to the FDTD analysis of planar microstrip circuits," *IEEE Trans. Microwave Theory Tech.*, vol. 42, pp. 2391–2398, Dec. 1994.

[6] M. A. Schamberger, S. Kosanovich, and R. Mittra, "Parameter extraction and correction for transmission lines and discontinuities using the finite-difference time-domain method," *IEEE Trans. Microwave Theory Tech.*, vol. 44, pp. 919–925, June 1996.

[7] R. Roy, A. Paulraj, and T. Kailath, "ESPRIT—A subspace rotation approach to estimation of parameters of cisoids in noise," *IEEE Trans. Acoust., Speech, Signal Processing*, vol. ASSP-34, pp. 1340–1342, Oct. 1986.

[8] J. P. Berenger, "A perfectly matched layer for the absorption of electromagnetic waves," *J. Comput. Phys.*, vol. 114, pp. 185–200, Oct. 1994.

[9] D. S. Katz, E. T. Thiele, and A. Taflove, "Validation and extension to three dimensions of the Berenger PML absorbing boundary condition for FD-TD meshes," *IEEE Microwave Guided Wave Lett.*, vol. 4, pp. 268–270, Aug. 1994.

[10] Y. Wang and H. Ling, "Extraction of higher order modes in open microstrip lines via FDTD and joint time-frequency analysis," *Microwave Opt. Technol. Lett.*, vol. 13, pp. 319–321, Dec. 1996.

[11] Y. Wang, "Multimode parameter extraction for general multiconduction transmission line via FDTD method and signal processing techniques," M.S. thesis, Dept. Elect. Comput. Eng., Univ. Texas at Austin, Aug. 1996.

[12] V. K. Tripathi and H. Lee, "Spectral domain computation of the apparent characteristic impedances and multiport parameters of multiple coupled microstrip lines," *IEEE Trans. Microwave Theory Tech.*, vol. 37, pp. 215–221, Jan. 1989.

[13] J. Moore, L. C. Trintinalia, H. Ling, and G. Xu, "Superresolved time-frequency processing of wide-band radar echo using ESPRIT," *Microwave Opt. Technol. Lett.*, vol. 9, pp. 17–19, May 1995.
[14] T. Kitazawa, "Variational method for multiconductor coupled striplines with stratified anisotropic media," *IEEE Trans. Microwave Theory Tech.*, vol. 37, pp. 484–491, Mar. 1989.
[15] G. Cano, F. Medina, and M. Horno, "Efficient spectral domain analysis of generalized multistrip lines in stratified media including thin, anisotropic, and lossy substrates," *IEEE Trans. Microwave Theory Tech.*, vol. 40, pp. 217–227, Feb. 1992.
[16] F. L. Mesa, G. Cano, F. Medina, R. Marques, and M. Horno, "On the quasi-TEM and full-wave approaches applied to coplanar multistrip on lossy dieletric layered media," *IEEE Trans. Microwave Theory Tech.*, vol. 40, pp. 524–531, Mar. 1992.

Yuanxun Wang (S'96) was born in Hubei, China, in 1973. He received the B.S.E.E. degree from the University of Science and Technology of China (USTC), Hefei, Anhui, in 1993, the M.S.E.E, degree from The University of Texas at Austin, in 1996, and is currently working toward the Ph.D. degree.

From 1993 to 1995, he was a Graduate Research Assistant at USTC, where his interests included numerical methods and developing millimeter-wave-level radar for industrial applications. In September 1995, he joined the Graduate School of The University of Texas at Austin, as a Research Assistant in the Department of Electrical and Computer Engineering, where his research has focused on the numerical simulation and signal post processing of various electromagnetic problems such as guided wave, scattering, and inverse synthetic-aperture radar imaging.

Hao Ling (S'83–M'86–SM'92) was born in Taichung, Taiwan, R.O.C., on September 26, 1959. He received the B.S. degree in electrical engineering and physics from the Massachusetts Institute of Technology, Cambridge, in 1982, and the M.S. and Ph.D. degrees in electrical engineering from the University of Illinois at Urbana-Champaign, in 1983 and 1986, respectively.

In September 1986, he joined the faculty of The University of Texas at Austin, and is currently a Professor of electrical and computer engineering. In 1982, he was associated with the IBM Thomas J. Watson Research Center, Yorktown Heights, NY, where he conducted low-temperature experiments in the Josephson Program. While in graduate school at the University of Illinois, he held a research assistantship in the Electromagnetics Laboratory. In 1987, he participated in the Summer Visiting Faculty Program at the Lawrence Livermore National Laboratory, CA. In 1990, he was a U.S. Air Force Summer Fellow at the Rome Air Development Center, Hanscom Air Force Base, MA. His research interests are in radar signature prediction, and computational techniques and radar signal analysis for scattering mechanism interpretation and target identification.

Dr. Ling is a recipient of the National Science Foundation Presidential Young Investigator Award in 1987, the NASA Certificate of Appreciation in 1991, and the Archie Straiton Junior Faculty Teaching Excellence Award in 1993.